Journal of Computational Science and Technology

Vol.2, No.2, 2008

Lattice Boltzmann Simulation of Two-Phase Viscoelastic Fluid Flows*

Masato YOSHINO**,***, Yasuyuki TORIUMI† and Masahiro ARAI**

** Department of Mechanical Systems Engineering, Shinshu University,
4–17–1 Wakasato, Nagano-shi, Nagano 380–8553, Japan

*** CREST, Japan Science and Technology Agency,
4–1–8 Honcho Kawaguchi, Saitama 332-0012, Japan

E-mail: masato@shinshu-u.ac.jp

† Department of Mechanical Systems Engineering, Graduate School of Science and Technology, Shinshu University,
4–17–1 Wakasato, Nagano-shi, Nagano 380–8553, Japan

Abstract

A lattice Boltzmann method (LBM) for two-phase viscoelastic fluid flows is proposed. The method is mainly an extension of the LBM for two-phase flows with large density differences proposed by Inamuro et al. [*Journal of Computational Physics* Vol.198, No.2 (2004), pp.628–644]. The viscoelastic effects are introduced by the constitutive equation based on the Maxwell model, which has a spring and a dashpot connected with each other in series. The method is applied to simulations of a drop under shear flow in viscoelastic fluids and of a bubble rising in viscoelastic fluids. In the simulation of drop deformation under shear flows, the effects of viscoelasticity on the deformation and orientation angle are evaluated. In the simulation of bubble rising in viscoelastic fluids, a cusp configuration at the trailing edge is investigated and compared with the theoretical prediction and other numerical results.

Key words : Lattice Boltzmann Method (LBM), Two Phase Flow, Viscoelastic Fluid, Shear Flow, Rising Bubble

1. Introduction

Recently, non-Newtonian fluid flows have attracted much attention in many scientific fields and engineering applications. Non-Newtonian fluids have several properties which are not observed in Newtonian fluids. In particular, viscoelasticity is one of them and regarded as an important property. Viscoelastic fluids show not only a viscous flow response to an imposed stress, as do Newtonian fluids, but also an elastic response. Viscoelastic fluid flows can be found in polymer blending for coating process, oil-and-water mixture in petroleum recovery, and so on.(1) In order to investigate dynamic behavior of the viscoelastic fluid flows, a numerical simulation is considered a very effective approach. However, complexity of the phenomena makes it difficult to develop numerical methods which incorporate nature of viscoelastic fluids.

Since the early 1990s, the lattice Boltzmann method (LBM) has been developed into an alternative and promising numerical scheme for simulating Newtonian viscous fluid flows and multiphase fluid flows.(2)–(5) In addition, the LBM has been also applied to non-Newtonian fluid flows, such as fluids with shear-dependent viscosity.(6)–(10) The advantages of the LBM are the simplicity of the algorithm, the accuracy of the mass and momentum conservations and the suitability for parallel computing. Thus, it is expected that the LBM has possibility of simulating the two-phase viscoelastic fluid flows. As for previous studies of viscoelastic fluid flows using the LBM, Giraud et al.(11),(12) developed two- and three- dimensional LB models of simple viscoelastic fluid flow. Ispolatov and Grant(13) proposed an LBM for viscoelastic fluid based on the Maxwell model for viscoelastic media. While their studies are confined

*Received 21 Mar., 2008 (No. 08-0199)
[DOI: 10.1299/jcst.2.330]

to one-component systems, Wagner et al.[14] extended the model by Giraud et al. to two-component systems, and investigated a cusped bubble rising in a viscoelastic fluid. Also, Onishi et al.[15] yielded an LB model for multi-component viscoelastic fluids using a discrete equation for elastic dumbbells. Their model is originated with the existing Shan and Chen model[16] for Newtonian fluids. In recent years, Inamuro et al.[17] have proposed a new LBM for two-phase flows. The great advantage of this method is that incompressible two-phase flows with large density ratio up to 1000 can be stably calculated using the method. Therefore, the method has been successfully applied to flow simulations of capillary waves,[17] binary droplet collisions[18] and bubble flows.[19]

In the present paper, an LBM for two-phase viscoelastic fluid flows is proposed, where elastic effects are incorporated into the above-mentioned LBM for two-phase flows with large density differences. The method is applied to simulations of a drop under shear flow in viscoelastic fluids and of a bubble rising in viscoelastic fluids. The results are compared with the theoretical prediction and other numerical results.

2. Numerical Method

Hereafter, as shown in Appendix, we use non-dimensional variables which are defined by a characteristic length L, a characteristic particle speed c, a characteristic time scale $t_0 = L/U$ where U is a characteristic flow speed, a reference order parameter ϕ_0 and a reference density ρ_0. In the LBM, a modeled fluid, composed of identical particles whose velocities are restricted to a finite set of M vectors $\boldsymbol{c}_i$ $(i = 1, 2, \ldots, M)$, is considered. The nine-velocity model $(M = 9)$ is used in the present paper. The velocity vectors of this model are $\boldsymbol{c}_1 = \boldsymbol{0}$, $\boldsymbol{c}_i = [\cos(\pi(i-2)/2), \sin(\pi(i-2)/2)]$ for $i = 2, 3, 4, 5$ and $\boldsymbol{c}_i = \sqrt{2}[\cos(\pi(i-11/2)/2), \sin(\pi(i-11/2)/2)]$ for $i = 6, 7, 8, 9$.

2.1. Elastic Stress Based on the Maxwell Model

In general, the Maxwell model, which has a spring and a dashpot connected with each other in series, is commonly used to express viscoelastic property. The Maxwell model for viscoelastic media links the elastic part of the stress tensor $\sigma^{\mathrm{el}}_{\alpha\beta}$ to the strain $\varepsilon_{\alpha\beta}$ in non-dimensional form as follows:[20]

$$\frac{\partial \varepsilon_{\alpha\beta}}{\partial t} = \frac{1}{G^{\mathrm{el}}}\frac{\partial \sigma^{\mathrm{el}}_{\alpha\beta}}{\partial t} + \frac{1}{\mathrm{Sh}}\frac{\sigma^{\mathrm{el}}_{\alpha\beta}}{\eta}, \tag{1}$$

where G^{el} is the shear modulus, η is the viscosity represented by a dashpot in the Maxwell model, $\mathrm{Sh}\,(= U/c)$ is the strouhal number and $\alpha, \beta = x, y$ (subscripts α and β represent Cartesian coordinates and the summation convention is used hereafter). The left-hand side of Eq. (1) indicates the rate of strain $\dot{\varepsilon}$ given by $\partial u_\alpha/\partial x_\beta + \partial u_\beta/\partial x_\alpha$, where u_α is the fluid velocity. Thus, the evolution of the stress tensor reads

$$\tau^{\mathrm{el}}\frac{\partial \sigma^{\mathrm{el}}_{\alpha\beta}}{\partial t} = -\sigma^{\mathrm{el}}_{\alpha\beta} + \eta\left(\frac{\partial u_\alpha}{\partial x_\beta} + \frac{\partial u_\beta}{\partial x_\alpha}\right), \tag{2}$$

where $\tau^{\mathrm{el}} = \mathrm{Sh}\,\eta/G^{\mathrm{el}}$ is the dimensionless stress relaxation time. Considering that the value of the stress is finite at $t = -\infty$, the differential equation is solved by the variation of parameter. Hence, the stress tensor at position $\boldsymbol{x}$ and at time t is given by

$$\sigma^{\mathrm{el}}_{\alpha\beta}(\boldsymbol{x}, t) = \frac{\eta}{\tau^{\mathrm{el}}}\int_{-\infty}^{t} \exp\left(-\frac{t-t'}{\tau^{\mathrm{el}}}\right)\dot{\varepsilon}(\boldsymbol{x}, t')\,dt'. \tag{3}$$

Taking the gradient of Eq. (3), the Maxwell elastic stress as a body force F_α is obtained by

$$F_\alpha(\boldsymbol{x}, t) = \frac{\eta}{\tau^{\mathrm{el}}}\int_{-\infty}^{t} \exp\left(-\frac{t-t'}{\tau^{\mathrm{el}}}\right)\nabla^2 u_\alpha(\boldsymbol{x}, t')\,dt', \tag{4}$$

where $\nabla^2 = \partial^2/\partial x_\alpha^2$ is the Laplace operator. Accordingly, Eq. (4) can be discretized with time step Δt as follows:[13]

$$F_\alpha(\boldsymbol{x}, t+\Delta t) = \left(1 - \frac{\Delta t}{\tau^{\mathrm{el}}}\right)F_\alpha(\boldsymbol{x}, t) + \frac{\eta \Delta t}{\tau^{\mathrm{el}}}\nabla^2 u_\alpha(\boldsymbol{x}, t). \tag{5}$$

As mentioned below, Eq. (5) representing the Maxwell viscoelastic effect is included into the evolution equation of the velocity distribution function as a body force in the original LBM for two-phase fluid flows.

2.2. Formulation

The present method is mainly based on the LBM for incompressible two-phase flows with large density differences proposed by Inamuro et al.[17] In the following, we assume two immiscible fluids composed of A- and B-phases where A-phase has a viscoelastic property based on the Maxwell model and B-phase has no elasticity. The physical space is divided into a square lattice, and the evolution of particle population at each lattice site is computed. Two particle velocity distribution functions, f_i and g_i, are used. The function f_i is used for the calculation of an order parameter which distinguishes two phases, and the function g_i is used for the calculation of a predicted velocity of the two-phase fluid without a pressure gradient. The evolution of the particle distribution functions $f_i(\boldsymbol{x}, t)$ and $g_i(\boldsymbol{x}, t)$ with velocity $\boldsymbol{c}_i$ at the point $\boldsymbol{x}$ and at time t is computed by the following equations:

$$f_i(\boldsymbol{x} + \boldsymbol{c}_i\Delta x, t + \Delta t) = f_i(\boldsymbol{x}, t) - \frac{1}{\tau_f}\left[f_i(\boldsymbol{x}, t) - f_i^{\mathrm{eq}}(\boldsymbol{x}, t)\right], \tag{6}$$

$$\begin{aligned} g_i(\boldsymbol{x} + \boldsymbol{c}_i\Delta x, t + \Delta t) &= g_i(\boldsymbol{x}, t) - \frac{1}{\tau_g}\left[g_i(\boldsymbol{x}, t) - g_i^{\mathrm{eq}}(\boldsymbol{x}, t)\right] \\ &+ 3E_i c_{i\alpha}\frac{1}{\rho}\left[\frac{\partial}{\partial x_\beta}\mu\left(\frac{\partial u_\beta}{\partial x_\alpha} + \frac{\partial u_\alpha}{\partial x_\beta}\right)\right]\Delta x \\ &+ 3E_i c_{i\alpha}\frac{1}{\rho}\left(\frac{\rho - \rho_{\mathrm{B}}}{\rho_{\mathrm{A}} - \rho_{\mathrm{B}}}\right)\left[\left(1 - \frac{\Delta t}{\tau^{\mathrm{el}}}\right)F_\alpha(\boldsymbol{x}, t - \Delta t) + \frac{\eta\Delta t}{\tau^{\mathrm{el}}}\nabla^2 u_\alpha(\boldsymbol{x}, t - \Delta t)\right]\Delta x, \end{aligned} \tag{7}$$

where f_i^{eq} and g_i^{eq} are equilibrium distribution functions, τ_f and τ_g are dimensionless single relaxation times, Δx is a spacing of the square lattice and the other variables, ρ, μ, $\boldsymbol{u}$, and constants E_i are defined below. The time step Δt is chosen as a time during which the particles travel the lattice spacing; it follows that $\Delta t = \mathrm{Sh}\Delta x$. The subscripts A and B represent quantities of A- and B-phases, respectively (the same rule is adopted hereafter).

The order parameter ϕ distinguishing two phases and the predicted velocity $\boldsymbol{u}^*$ of the two-phase fluid are defined in terms of the two particle velocity distribution functions as follows:

$$\phi = \sum_{i=1}^{9} f_i, \tag{8}$$

$$\boldsymbol{u}^* = \sum_{i=1}^{9} g_i \boldsymbol{c}_i. \tag{9}$$

The equilibrium distribution functions f_i^{eq} and g_i^{eq} in Eqs. (6) and (7) are given by

$$\begin{aligned} f_i^{\mathrm{eq}} &= H_i\phi + F_i\left[p_0 - \kappa_f\phi\nabla^2\phi\right] + E_i\phi\left(3u_\alpha c_{i\alpha} - \frac{3}{2}u_\alpha u_\alpha + \frac{9}{2}u_\alpha u_\beta c_{i\alpha}c_{i\beta}\right) \\ &+ E_i\kappa_f G_{\alpha\beta}(\phi)c_{i\alpha}c_{i\beta}, \end{aligned} \tag{10}$$

$$\begin{aligned} g_i^{\mathrm{eq}} &= E_i\left[1 + 3u_\alpha c_{i\alpha} - \frac{3}{2}u_\alpha u_\alpha + \frac{9}{2}u_\alpha u_\beta c_{i\alpha}c_{i\beta} + \frac{3}{2}\left(\tau_g - \frac{1}{2}\right)\Delta x\left(\frac{\partial u_\beta}{\partial x_\alpha} + \frac{\partial u_\alpha}{\partial x_\beta}\right)c_{i\alpha}c_{i\beta}\right] \\ &+ E_i\frac{\kappa_g}{\rho}G_{\alpha\beta}(\rho)c_{i\alpha}c_{i\beta} - \frac{1}{2}F_i\frac{\kappa_g}{\rho}|\nabla\rho|^2, \end{aligned} \tag{11}$$

where

$$\left.\begin{aligned} &E_1 = 4/9,\ E_2 = E_3 = E_4 = E_5 = 1/9, \\ &E_6 = E_7 = E_8 = E_9 = 1/36, \\ &F_1 = -5/3, \quad F_i = 3E_i \ \ (i = 2, 3, \ldots, 9), \\ &H_1 = 1, \quad H_i = 0 \ \ (i = 2, 3, \ldots, 9), \end{aligned}\right\} \tag{12}$$

and

$$G_{\alpha\beta}(\phi) = \frac{9}{2}\frac{\partial\phi}{\partial x_\alpha}\frac{\partial\phi}{\partial x_\beta} - \frac{9}{4}\frac{\partial\phi}{\partial x_\gamma}\frac{\partial\phi}{\partial x_\gamma}\delta_{\alpha\beta}. \tag{13}$$

In the above equations, κ_f and κ_g are constant parameters determining the width of the interface and the strength of the surface tension, respectively, and $\delta_{\alpha\beta}$ is the Kronecker delta. In Eq. (10), p_0 is given by

$$p_0 = \phi T\frac{1}{1-b\phi} - a\phi^2, \tag{14}$$

where a, b and T are free parameters determining the maximum and minimum values of ϕ. The following finite-difference approximations are used to calculate the gradient and the divergence of the scalar variable ψ (= u_β, ϕ, ρ) in Eqs. (7), (10), (11) and (13):

$$\frac{\partial\psi}{\partial x_\alpha} \approx \frac{1}{6\Delta x}\sum_{i=2}^{9} c_{i\alpha}\psi(\boldsymbol{x}+\boldsymbol{c}_i\Delta x), \tag{15}$$

$$\nabla^2\psi \approx \frac{1}{3(\Delta x)^2}\left[\sum_{i=2}^{9}\psi(\boldsymbol{x}+\boldsymbol{c}_i\Delta x) - 8\psi(\boldsymbol{x})\right]. \tag{16}$$

The density in the interface is obtained using the cut-off values of the order parameter, ϕ_{A}^* and ϕ_{B}^*, for A- and B-phases with the following relation:

$$\rho = \begin{cases} \rho_{\mathrm{B}}, & \phi < \phi_{\mathrm{B}}^*, \\ \dfrac{\Delta\rho}{2}\left[\sin\left(\dfrac{\phi-\overline{\phi^*}}{\Delta\phi^*}\pi\right)+1\right]+\rho_{\mathrm{B}}, & \phi_{\mathrm{B}}^* \le \phi \le \phi_{\mathrm{A}}^*, \\ \rho_{\mathrm{A}}, & \phi > \phi_{\mathrm{A}}^*, \end{cases} \tag{17}$$

where $\Delta\rho = \rho_{\mathrm{A}} - \rho_{\mathrm{B}}$, $\Delta\phi^* = \phi_{\mathrm{A}}^* - \phi_{\mathrm{B}}^*$, $\overline{\phi^*} = (\phi_{\mathrm{A}}^* + \phi_{\mathrm{B}}^*)/2$. The viscosity μ in the interface is obtained by

$$\mu = \frac{\rho-\rho_{\mathrm{B}}}{\rho_{\mathrm{A}}-\rho_{\mathrm{B}}}(\mu_{\mathrm{A}}-\mu_{\mathrm{B}}) + \mu_{\mathrm{B}}, \tag{18}$$

where μ_{A} implies the viscosity which derives from the collision process in the original LBM. Hence, it is noted that the viscous part coming from the Maxwell model should be included into the effective viscosity of the viscoelastic fluid (A-phase). Also, the surface tension σ is given by

$$\sigma = \kappa_g\int_{-\infty}^{\infty}\left(\frac{\partial\rho}{\partial\xi}\right)^2 d\xi, \tag{19}$$

with ξ being the coordinate normal to the interface.[21),(22)]

Since $\boldsymbol{u}^*$ is not divergence free ($\nabla\cdot\boldsymbol{u}^* \neq 0$) in general, the correction of $\boldsymbol{u}^*$ is required. The current velocity $\boldsymbol{u}$ which satisfies the continuity equation ($\nabla\cdot\boldsymbol{u} = 0$) can be obtained using the following equations:

$$\mathrm{Sh}\frac{\boldsymbol{u}-\boldsymbol{u}^*}{\Delta t} = -\frac{\nabla p}{\rho}, \tag{20}$$

$$\nabla\cdot\left(\frac{\nabla p}{\rho}\right) = \mathrm{Sh}\frac{\nabla\cdot\boldsymbol{u}^*}{\Delta t}. \tag{21}$$

In order to solve the Poisson equation (21), the following evolution equation of the velocity distribution function h_i is used for the calculation of the pressure p:

$$h_i^{n+1}(\boldsymbol{x}+\boldsymbol{c}_i\Delta x) = h_i^n(\boldsymbol{x}) - \frac{\rho}{1+\rho/2}\left[h_i^n(\boldsymbol{x}) - E_i p^n(\boldsymbol{x})\right] - \frac{1}{3}E_i\frac{\partial u_\alpha^*}{\partial x_\alpha}\Delta x, \tag{22}$$

where n is the number of iterations. The pressure is obtained by

$$p = \sum_{i=1}^{9} h_i. \tag{23}$$

The iteration of Eq. (22) is repeated until $\left|p^{n+1}-p^n\right|/\rho < \epsilon$ is satisfied in the whole domain, where ϵ means a convergence criterion.

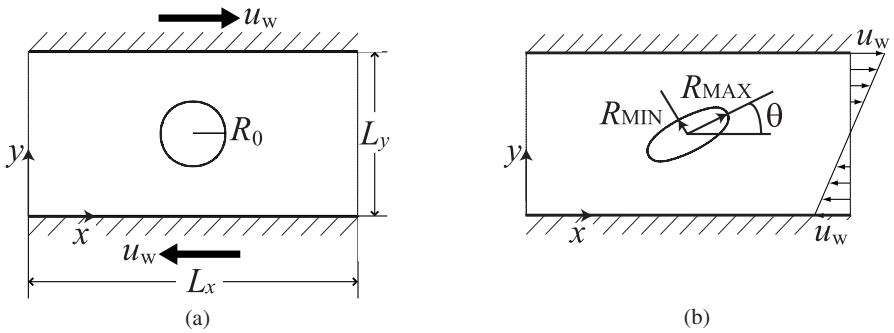

Fig. 1 Deformation of a drop in shear flows: (a) geometry and coordinates; (b) definition of R_{MAX}, R_{MIN} and θ.

3. Numerical Examples

3.1. Dynamics of a Drop under Shear Flow in Viscoelastic Fluids

Dynamic behavior of a drop under shear flow in viscoelastic fluids is simulated using the present method. As shown in Fig. 1(a), a rectangular domain with $L_x \times L_y = 128\Delta x \times 64\Delta x$ is considered. The domain is filled with a viscoelastic matrix fluid (A-phase), and a single Newtonian drop (B-phase) with initial radius R_0 is placed at the center of the domain. At time $t = 0$, the upper and lower walls are suddenly moved in opposite directions ($\pm$ x-directions) with a speed u_w. The no-slip boundary condition is used on the moving walls, and the periodic boundary condition is used on the sides of the domain.

As shown in Ref. (23), the main dimensionless parameters for this problem are the following two quantities. One is the capillary number $\mathrm{Ca} = \mu_A^* \Gamma R_0/\sigma$, where $\mu_A^* = \mu_A + \eta\Delta t/\tau^{el}$ is the effective viscosity and $\Gamma = 2u_w/L_y$ is the imposed shear rate, and the other is a parameter representing the ratio of elastic to interfacial stresses, $N = N_1 R_0/(2\sigma)$, where $N_1 = 2\eta\Gamma\Delta t/\tau^{el}$ is the first normal stress difference in the matrix fluid. According to Ref. (24), effects of fluid elasticity on drop shape can be observable when $\mathrm{Ca}^2 \sim N$ in order-of-magnitude sense. Therefore, order of a non-dimensional ratio $P = N/\mathrm{Ca}^2$ is set to unity in the simulations. The parameters in Eq. (14) are $a = 1$, $b = 6.7$ and $T = 3.5 \times 10^{-2}$; it follows that the maximum and minimum values of the order parameter are $\phi_{max} = 9.714 \times 10^{-2}$ and $\phi_{min} = 1.134 \times 10^{-2}$. The cut-off values of the order parameter are $\phi_A^* = 9.20 \times 10^{-2}$ and $\phi_B^* = 1.50 \times 10^{-2}$. The other parameters are fixed at $\tau^{el} = 1 \times 10^{-4}$, $\tau_f = 1$, $\tau_g = 1$, $\epsilon = 10^{-6}$, $R_0 = 12\Delta x$, $\rho_A = 1.1$, $\rho_B = 1$ ($\rho_A/\rho_B = 1.1$), $\mu_B = 0.1\Delta x$ and $\kappa_f = 0.5(\Delta x)^2$. Note that the parameter κ_g is changed so as to give different values of the surface tension σ. Also, in all cases, the effective viscosity μ_A^* is fixed at $0.3\Delta x$, though μ_A and η are changed separately. The deformation is evaluated by the Taylor's deformation parameter[25] $D = (R_{MAX} - R_{MIN})/(R_{MAX} + R_{MIN})$ and the orientation angle θ, where R_{MAX} and R_{MIN} are the major and minor axes of the deformed ellipsoidal drop, respectively, as defined in Fig. 1(b). It should be noted that the orientation angle θ has unit of degree.

First, unsteady behavior of the drop under shear flow is investigated for different P-values at a constant capillary number. Figure 2 shows time evolution of the deformation parameter D and orientation angle θ at $\mathrm{Ca} = 0.26$. Note that the horizontal axis indicates the dimensionless time $t^* = tu_w/L_y$. In all cases, the deformation parameter D, which initially increases rapidly owing to the imposed shear flow, overshoots around $t^* = 1.3 \sim 1.5$ and then approaches the equilibrium state. It is found that the equilibrium values of D are almost constant in spite of different viscoelastic parameters, though a little larger value can be seen for $P = 2.4$. The orientation angle θ, on the other hand, decreases with time at the early stage and then converges to respective equilibrium values. Also, it is found that the equilibrium value becomes smaller as the P-value increases. These tendencies are in qualitative agreement with the results by Onishi et al.[15]

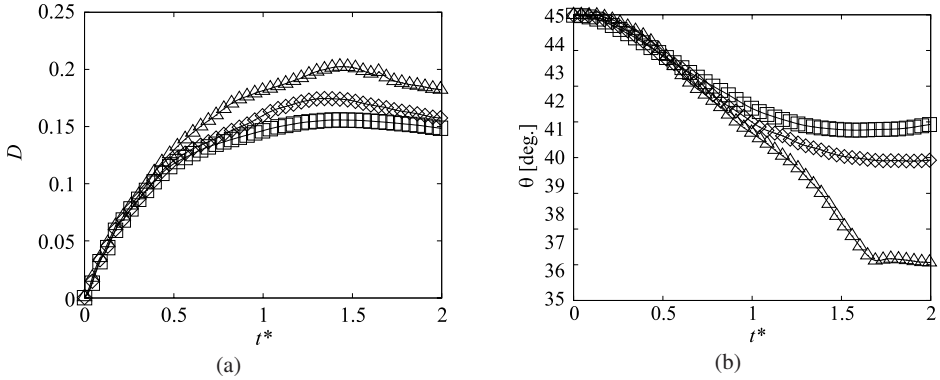

(a) (b)

Fig. 2 Time variations of drop characteristics: (a) deformation parameter D; (b) orientation angle θ: □, $P = 0.6$; ◇, $P = 1.2$; △, $P = 2.4$. The capillary number is 0.26 ($t^* = tu_w/L_y$).

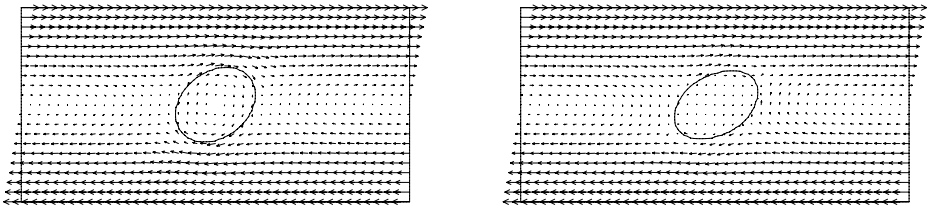

(a) (b)

Fig. 3 Velocity fields and deformation of a droplet: (a) in Newtonian fluid ($P = 0$); (b) in viscoelastic fluid ($P = 2.4$). The capillary number is 0.26.

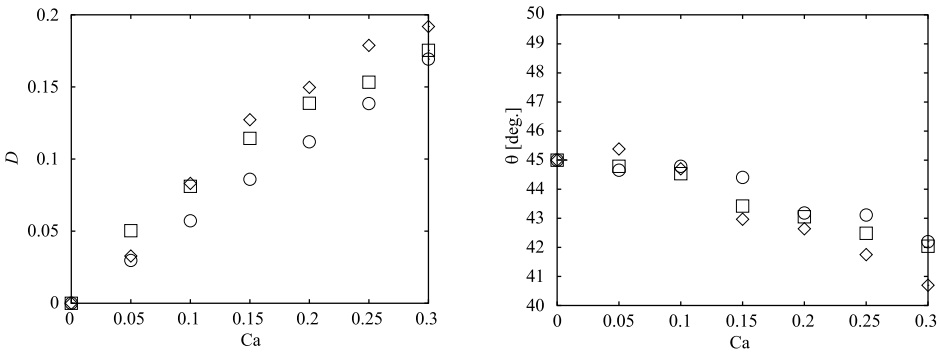

(a) (b)

Fig. 4 Plots of (a) deformation parameter D and (b) orientation angle θ obtained at steady state against different capillary numbers: ○, $P = 0$; □, $P = 0.6$; ◇, $P = 1.2$.

Next, viscoelastic effects of the matrix fluid on the drop deformation are examined. Figure 3 shows steady-state results of velocity vectors and drop shape in different matrices, namely, (a) a Newtonian fluid and (b) a viscoelastic fluid for $P = 2.4$ at a constant capillary number (Ca = 0.26). It can be seen that although the drops in both cases have almost the same elliptic shape, the drop in the viscoelastic matrix is more oriented toward the flow direction than that in the Newtonian matrix.

Finally, the effects of the capillary number on the drop deformation are investigated. Figure 4 demonstrates the relation of (a) deformation parameter D and (b) orientation angle θ to the capillary number. The deformation parameter increases almost linearly and the orientation angle slightly decreases with the capillary number.

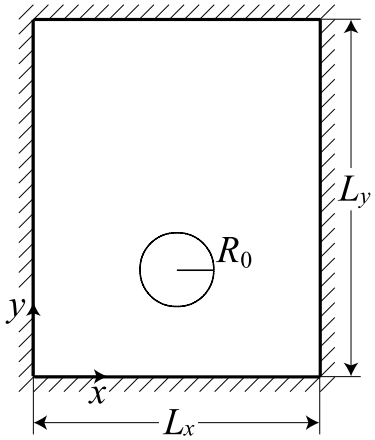

Fig. 5 Problem of a Newtonian bubble rising in viscoelastic fluid and initial state of the bubble.

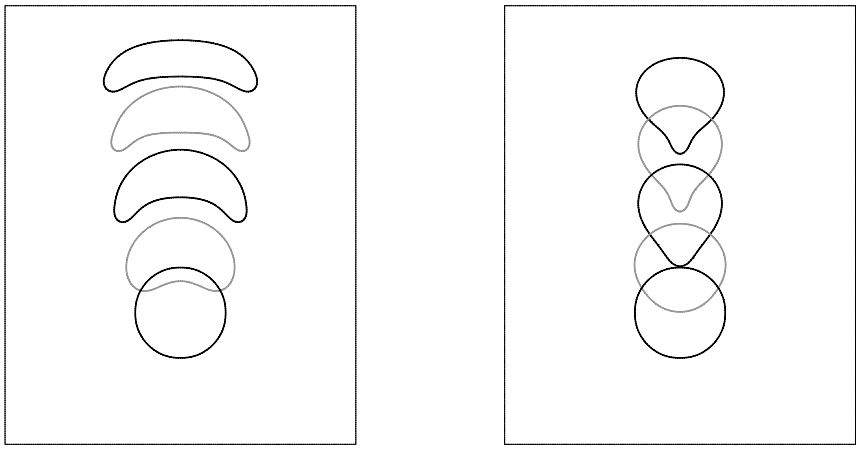

(a) (b)

Fig. 6 Time evolution of bubble shape for $R_0 = 20\Delta x$ and $\sigma = 8.89 \times 10^{-5}\Delta x$ [$\kappa_g = 1 \times 10^{-4}(\Delta x)^2$]: (a) in Newtonian fluid at Ca = 4.48 and Re = 3.97; (b) in viscoelastic fluid at Ca = 3.72 and Re = 3.29.

3.2. Dynamics of a Bubble Rising in Viscoelastic Fluids

Dynamic behavior of a bubble rising in viscoelastic fluids is simulated using the present method. As shown in Fig. 5, a rectangular domain with $L_x \times L_y = 160\Delta x \times 200\Delta x$ is considered. In the calculations, the gravitational force is assumed by adding the term $-3E_i c_{iy}(1 - (\rho_A/\rho))g\Delta x$, where g is the gravitational acceleration, to the right-hand side of Eq. (7). The domain is filled with a viscoelastic fluid (A-phase), and a single Newtonian bubble (B-phase) with the center of an initial radius R_0 is placed at $(x/L_x, y/L_y) = (0.5, 0.3)$ and released at time $t = 0$. The no-slip boundary condition is used on all the walls. The dimensionless parameters are the capillary number $\mathrm{Ca} = V\mu_A^*/\sigma$ and the Reynolds number $\mathrm{Re} = \rho_A V R_0/\mu_A^*$, where V is the mass-averaged vertical velocity of the rising bubble defined by[26]

$$V = \frac{\int(\rho_A - \rho)u_y\, dS}{\int(\rho_A - \rho)\, dS}, \tag{24}$$

where dS is the area element. The values of the parameters, a, b, T, ρ_{max}, ρ_{min}, ϕ_A^*, ϕ_B^*, τ_f, τ_g and ϵ are the same as in the previous problem. The other parameters are fixed at $\tau^{el} = 16.7$, $\rho_A = 5$, $\rho_B = 1$ ($\rho_A/\rho_B = 5$), $\mu_B = 2 \times 10^{-3}\Delta x$, $\kappa_f = 1.5(\Delta x)^2$ and $g\Delta x = 2.83 \times 10^{-6}$. The parameter κ_g is changed so as to give different values of σ, and in all cases, μ_A^* is fixed at $1.2 \times 10^{-4}\Delta x$ in spite of changing the values of μ_A and η separately.

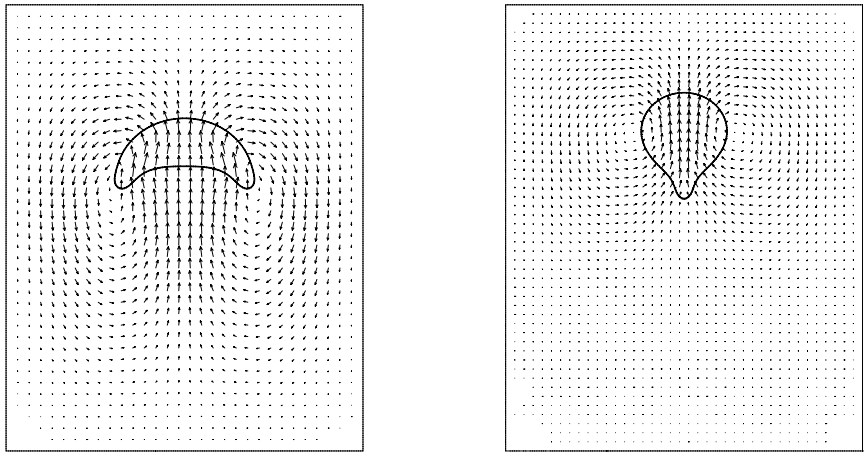

Fig. 7 Velocity vectors and bubble shape for $R_0 = 20\Delta x$ and $\sigma = 8.89 \times 10^{-5}\Delta x$ [$\kappa_g = 1 \times 10^{-4}(\Delta x)^2$]: (a) in Newtonian fluid at $t^* = 3.98$; (b) in viscoelastic fluid at $t^* = 4.30$ ($t^* = tV/R_0$).

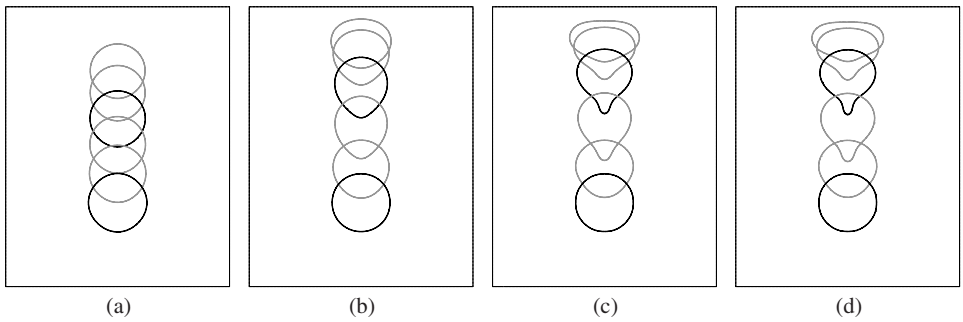

Fig. 8 Deformation of bubble rising in viscoelastic fluid for different capillary numbers: (a) Ca = 3.28×10^{-2}; (b) Ca = 4.63×10^{-1}; (c) Ca = 4.96; (d) Ca = 49.5. The initial radius of the bubble is fixed at $R_0 = 20\Delta x$.

We first compare differences in the behavior of rising bubbles in a Newtonian fluid and in a viscoelastic fluid. Figure 6 shows time evolution of behavior of the bubble with $R_0 = 20\Delta x$ and $\sigma = 8.89 \times 10^{-5}\Delta x$ [$\kappa_g = 1 \times 10^{-4}(\Delta x)^2$] in these cases. The values of the dimensionless parameters are Ca = 4.48 and Re = 3.97 in the Newtonian fluid and Ca = 3.72 and Re = 3.29 in the viscoelastic fluid. The bubbles go up due to the buoyancy force in both cases, but the shapes of the bubbles are quite different from each other. In the Newtonian case, the bubble is deformed into a concave shape on the lower side, and finally becomes an umbrella-like shape. In the viscoelastic case, on the other hand, the bubble is elongated in the vertical direction and forms a cusp at the trailing edge, as observed in experiments.[27] Moreover, Fig. 7 shows results of velocity vectors and bubble shape in these cases. It is seen that relatively large-scale circulatory flows are induced symmetrically around the bubble in each case.

We next investigate the effects of the capillary number on bubble shapes rising in the viscoelastic fluid. In the calculations, the parameter κ_g is changed so that the capillary number becomes $3.28 \times 10^{-2} \leq \mathrm{Ca} \leq 49.5$. The initial radius is fixed at $R_0 = 20\Delta x$. Figure 8 shows the calculated results of bubble shape for different capillary numbers. It is seen that for smaller capillary numbers, the bubble rises while keeping the initial round shape. This feature is in good agreement with other numerical results[26] by the finite element method. Moreover, it is expected from the figures that the bubble can form a cusp when Ca is approximately of $O(1)$.

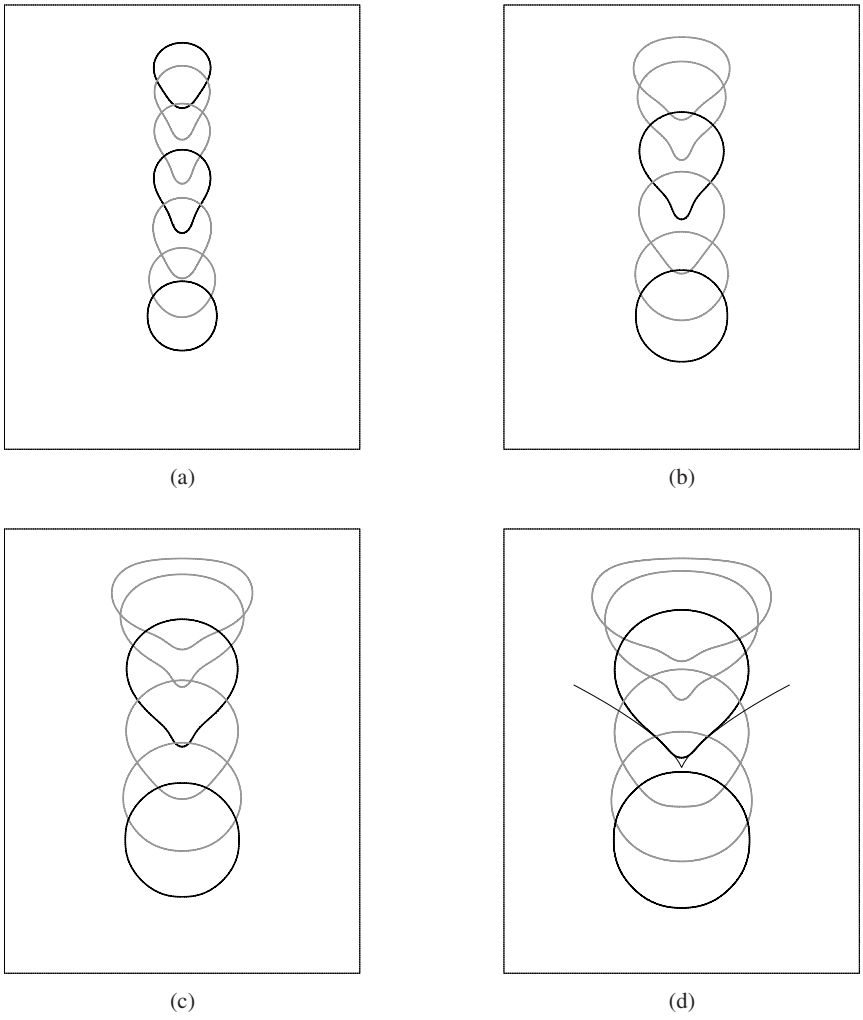

Fig. 9 Deformation of bubble rising in viscoelastic fluid for different initial sizes: (a) $R_0 = 15\Delta x$; (b) $R_0 = 20\Delta x$; (c) $R_0 = 25\Delta x$; (d) $R_0 = 30\Delta x$. The capillary numbers are Ca ≈ 3 in all cases. The curve to the predicted functional form of $|x|^{2/3}$ is also shown in (d).

We finally investigate the cusp configuration in the viscoelastic fluid. Figure 9 shows the bubble behavior for different initial sizes, $R_0 = 15\Delta x$, $20\Delta x$, $25\Delta x$ and $30\Delta x$, with the capillary number being of $O(1)$, in fact, Ca ≈ 3. As the initial size of the bubble increases, the bottom edge becomes sharper and the cusp configuration is clearly observed. In particular, for the case of (d) $R_0 = 30\Delta x$, it is found that the cusp can be fitted to the functional form $|x|^{2/3}$ predicted by Joseph et al.[28] for a two-dimensional cusp created by the flow induced in two counter-rotating cylinders.

4. Concluding Remarks

A lattice Boltzmann method (LBM) for two-phase viscoelastic fluid flows has been proposed. The method is applied to simulations of a drop under shear flow in viscoelastic fluids and of a bubble rising in viscoelastic fluids. It is found that the present method is successful in the two-dimensional simulations, but the extension to three-dimensions will enable us to make quantitative comparison of our results with available experimental data as well as other numerical results.

Finally, according to experimental studies by Liu et al.[27] and by Soto et al.,[29] velocity jump and negative wake can be seen in the problem of a rising bubble in viscoelastic fluids,

though they are not discussed in the present paper. Therefore, further investigation into these peculiar phenomena is also required in future work.

Acknowledgements

This work was supported by the Grant-in-Aid for Young Scientists (B) [No.18760121] of the Ministry of Education, Culture, Sports, Science and Technology, Japan (MEXT) and of the Japan Society for the Promotion of Science (JSPS).

Appendix Non-dimensional variables

As in Ref. (17), we use the following non-dimensional variables which are defined by a characteristic length L, a characteristic particle speed c, a characteristic time scale $t_0 = L/U$ where U is a characteristic flow speed, a reference order parameter ϕ_0 and a reference density ρ_0:

$$\left.\begin{array}{lll}
\hat{\boldsymbol{c}}_i = \boldsymbol{c}_i/c, & \hat{\boldsymbol{x}} = \boldsymbol{x}/L, & \hat{t} = t/t_0, \\
\hat{\boldsymbol{\sigma}}^{\mathrm{el}} = \boldsymbol{\sigma}^{\mathrm{el}}/(\rho_0 c^2), & \hat{G}^{\mathrm{el}} = G^{\mathrm{el}}/(\rho_0 c^2), & \hat{\eta} = \eta/(\rho_0 cL), \\
\hat{\dot{\varepsilon}} = \dot{\varepsilon}\, t_0, & \hat{\tau}^{\mathrm{el}} = \tau^{\mathrm{el}}/t_0, & \hat{\boldsymbol{F}} = \boldsymbol{F}/(\rho_0 c^2 L^2), \\
\hat{f}_i = f_i/\phi_0, & \hat{g}_i = g_i/\rho_0, & \hat{h}_i = h_i/(\rho_0 c^2), \\
\hat{\phi} = \phi/\phi_0, & \hat{\rho} = \rho/\rho_0, & \\
\hat{\boldsymbol{u}} = \boldsymbol{u}/c, & \hat{p} = p/(\rho_0 c^2), & \\
\hat{\mu} = \mu/(\rho_0 cL), & \hat{\sigma} = \sigma/(\rho_0 c^2 L), & \hat{g} = gL/c^2.
\end{array}\right\}. \qquad \text{(A.1)}$$

Note that the circumflex representing 'non-dimensional' in Eq. (A.1) is omitted in the paper for simplicity.

References

(1) Bird, R.B., Armstrong, R.C. and Hassager, O., *Dynamics of Polymeric Liquids*, Vol.2, 2nd Edition, (1987), John Wiley & Sons Ltd.

(2) Rothman, D.H. and Zaleski, S., *Lattice-Gas Cellular Automata*, (1997), Cambridge University Press.

(3) Chen, S. and Doolen, G.D., Lattice Boltzmann Method for Fluid Flows, *Annual Review Fluid Mechanics* Vol.30 (1998), pp.329–364.

(4) Succi, S., *The Lattice Boltzmann Equation for Fluid Dynamics and Beyond*, (2001), Oxford University Press.

(5) Inamuro, T., Lattice Boltzmann Methods for Viscous Fluid Flows and for Two-Phase Fluid Flows, *Fluid Dynamic Research* Vol.38, No.9 (2006), pp.641–659.

(6) Aharonov, E. and Rothman, D.H., Non-Newtonian Flow (Through Porous Media): A Lattice-Boltzmann Method, *Geophysical Research Letters* Vol.20, No.8 (1993), pp.679–682.

(7) Boek, E.S., Chin, J. and Coveney, P.V., Lattice Boltzmann Simulation of the Flow of Non-Newtonian Fluids in Porous Media, *International Journal of Modern Physics B* Vol.17, Nos.1–2 (2003), pp.99–102.

(8) Gabbanelli, S., Drazer, G. and Koplik, J., Lattice Boltzmann Method for Non-Newtonian (Power-Law) Fluids, *Physical Review E* Vol.72 (2005), 046312.

(9) Sullivan, S.P., Gladden, L.F. and Johns, M.L., Simulation of Power-Law Fluid Flow through Porous Media Using Lattice Boltzmann Techniques, *Journal of Non-Newtonian Fluid Mechanics* Vol.133, Nos.2–3 (2006), pp.91–98.

(10) Yoshino, M., Hotta, Y., Hirozane, T. and Endo, M., A Numerical Method for Incompressible Non-Newtonian Fluid Flows Based on the Lattice Boltzmann Method, *Journal of Non-Newtonian Fluid Mechanics* Vol.147, Nos.1–2 (2007), pp.69–78.

(11) Giraud, L., d'Humières, D. and Lallemand, P., A Lattice-Boltzmann Model for Visco-Elasticity, *International Journal of Modern Physics C* Vol.8, No.4 (1997), pp.805–815.

(12) Giraud, L., d'Humières, D. and Lallemand, P., A Lattice Boltzmann Model for Jeffreys Viscoelastic Fluid, *Europhysics Letters* Vol.42, No.6 (1998), pp.625–630.
(13) Ispolatov, I. and Grant, M., Lattice Boltzmann Method for Viscoelastic Fluids, *Physical Review E* Vol.65 (2002), 056704.
(14) Wagner, A.J., Giraud, L. and Scott, C.E., Simulation of a Cusped Bubble Rising in a Viscoelastic Fluid with a New Numerical Method, *Computer Physics Communications* Vol.129, Nos.1–3 (2000), pp.227–232.
(15) Onishi, J., Chen, Y. and Ohashi, H., Dynamic Simulation of Multi-Component Viscoelastic Fluids Using the Lattice Boltzmann Method, *Physica A* Vol.362, No.1 (2006), pp.84–92.
(16) Shan, X. and Chen, H., Lattice Boltzmann Model for Simulating Flows with Multiple Phases and Components, *Physical Review E* Vol.47 (1993), pp.1815–1819.
(17) Inamuro, T., Ogata, T., Tajima, S. and Konishi, N., A Lattice Boltzmann Method for Incompressible Two-Phase Flows with Large Density Differences, *Journal of Computational Physics* Vol.198, No.2 (2004), pp.628–644.
(18) Inamuro, T., Tajima, S. and Ogino, F., Lattice Boltzmann Simulation of Droplet Collision Dynamics, *International Journal of Heat and Mass Transfer* Vol.47, No.21 (2004), pp.4649–4657.
(19) Inamuro, T., Ogata, T. and Ogino, F., Numerical Simulation of Bubble Flows by the Lattice Boltzmann Method, *Future Generation Computer Systems* Vol.20, No.6 (2004), pp.959–964.
(20) Drozdov, A.D., *Finite Elasticity and Viscoelasticity : A Course in the Nonlinear Mechanics of Solids*, (1996), pp.247–267, World Scientific Publishing Co. Pte. Ltd.
(21) Rowlinson, J.S. and Widom, B., *Molecular Theory of Capillarity*, (1989), pp.50–68, Clarendon Press.
(22) Inamuro, T., Konishi, N. and Ogino, F., A Galilean Invariant Model of the Lattice Boltzmann Method for Multiphase Fluid Flows Using Free-Energy Approach, *Computer Physics Communications* Vol.129, Nos.1–3 (2000), pp.32–45.
(23) Greco, F., Drop Deformation for Non-Newtonian Fluids in Slow Flows, *Journal of Non-Newtonian Fluid Mechanics* Vol.107, Nos.1–3 (2002), pp.111–131.
(24) Guido, S., Simeone, M. and Greco, F., Deformation of a Newtonian Drop in a Viscoelastic Matrix under Steady Shear Flow: Experimental Validation of Slow Flow Theory, *Journal of Non-Newtonian Fluid Mechanics* Vol.114, No.1 (2003), pp.65–82.
(25) Taylor, G.I., The Viscosity of a Fluid Containing Small Drops of Another Fluid, *Proceedings of the Royal Society of London. Series A, Mathematical and Physical Sciences* Vol.138, No.834 (1932), pp.41–48.
(26) Pillapakkam, S.B. and Singh, P., A Level-Set Method for Computing Solutions to Viscoelastic Two-Phase Flow, *Journal of Computational Physics* Vol.174, No.2 (2001), pp.552–578.
(27) Liu, Y.J., Liao, T.Y. and Joseph, D.D., A Two-Dimensional Cusp at the Trailing Edge of an Air Bubble Rising in a Viscoelastic Liquid, *Journal of Fluid Mechanics* Vol.304 (1995), pp.321–342.
(28) Joseph, D.D., Nelson, J.J., Renardy, M. and Renardy, Y., Two-Dimensional Cusped Interfaces, *Journal of Fluid Mechanics* Vol.223 (1991), pp.383–409.
(29) Soto, E., Goujon, C., Zenit, R. and Manero, O., A Study of Velocity Discontinuity for Single Air Bubbles Rising in an Associative Polymer, *Physics of Fluids* Vol.18, No.12 (2006), 121510.